Determination of the spin orbit coupling and crystal field splitting in wurtzite InP by polarization resolved photoluminescence

Nicolas Chauvin, Amaury Mavel, Ali Jaffal, Gilles Patriarche, Michel Gendry

Determination of the spin orbit coupling and crystal field splitting in wurtzite InP by polarization resolved photoluminescence

Nicolas Chauvin[1,a)], Amaury Mavel[1,2], Ali Jaffal[1,2], Gilles Patriarche[3], Michel Gendry[2]

[1]*Université de Lyon, Institut des Nanotechnologies de Lyon (INL)-UMR5270-CNRS, INSA-Lyon, 7 avenue Jean Capelle, 69621 Villeurbanne, France.*

[2] *Université de Lyon, Institut des Nanotechnologies de Lyon (INL)-UMR5270-CNRS, Ecole Centrale de Lyon, 36 avenue Guy de Collongue, 69134 Ecully, France.*

[3] *Centre de Nanosciences et de Nanotechnologies – site Marcoussis, UMR 9001 CNRS, Univ. Paris Sud, Univ. Paris-Saclay, Route de Nozay, 91460 Marcoussis, France.*

ABSTRACT

Excitation photoluminescence spectroscopy is usually used to extract the crystal field splitting (Δ_{CR}) and spin orbit coupling (Δ_{SO}) parameters of wurtzite (Wz) InP nanowires (NWs). However, the equations expressing the valence band splitting are symmetric with respect to these two parameters and a choice $\Delta_{CR}>\Delta_{SO}$ or $\Delta_{CR}<\Delta_{SO}$ has to be taken into account in order to assign the numerical values. To solve this issue, polarization resolved micro-photoluminescence was performed on vertically aligned and untapered Wz InP NWs grown on silicon. The experimental results combined with a theoretical model and FDTD calculations allow us to conclude that $\Delta_{CR}>\Delta_{SO}$ in Wz InP.

[a)]Author to whom correspondence should be addressed. Electronic mail: nicolas.chauvin@insa-lyon.fr

In recent years, several groups have experimentally investigated the band structure properties of wurtzite (Wz) InP nanowires (NWs) to gain access to parameters such as the band-gap and Varshni parameters,[1] the effective masses,[2] the deformation potentials,[3] the dipole orientation [4] or the Young modulus.[5] However some band structure parameters are still not very well-known. In the Wz phase, the degeneracy of the first three valence bands (usually labeled A, B and C bands) is lifted (Figure 1.a). Within the quasi-cubic approximation these valence band splittings are a consequence of the spin orbit coupling (Δ_{SO}) and the crystal field splitting (Δ_{CR}). One of the open questions is to determine if the spin orbit coupling (Δ_{SO}) parameter is bigger or smaller than the crystal field splitting (Δ_{CR}). In the literature, the experimental values of these two parameters are usually deduced from optical measurements such as photoluminescence (PL) or PL excitation (PLE). The A, B and C transitions of InP Wz are identified and the Δ_{SO} and Δ_{CR} are deduced from the energy levels of these transitions using the equations[6]:

$$\Delta E_{AB} = \frac{\Delta_{SO} + \Delta_{CR}}{2} - \sqrt{\left(\frac{\Delta_{SO} + \Delta_{CR}}{2}\right)^2 - \frac{2}{3}\Delta_{SO}\Delta_{CR}} \quad (1)$$

$$\Delta E_{AC} = \frac{\Delta_{SO} + \Delta_{CR}}{2} + \sqrt{\left(\frac{\Delta_{SO} + \Delta_{CR}}{2}\right)^2 - \frac{2}{3}\Delta_{SO}\Delta_{CR}} \quad (2)$$

where ΔE_{AB} (ΔE_{AC}) is the energy difference between A and B (A and C) transitions. The main concern with this method is the fact that the two equations are symmetric in regards of the Δ_{SO} and Δ_{CR} values. As a consequence, a couple of numbers can be extracted but an assumption, $\Delta_{CR} > \Delta_{SO}$ or the opposite one, has to be chosen to attribute the experimental values to the intrinsic parameters of the material. As a consequence, some published works, such as in the work of M.H. *Hadj Alouane et al*,[7] have considered that Δ_{CR} is bigger than Δ_{SO} whereas the opposite choice has been taken in the work of S. *Perera et al*.[8]

To conclude on this issue, we have to focus on properties related to Δ_{SO} and Δ_{CR} but not on a symmetrical way. One interesting possibility is to investigate the polarization resolved PL of Wz InP NWs. The ratio of PL intensity polarized parallel to the NW axis (z axis) over the perpendicular one (x axis) is equal to $I_z/I_x = \beta d_{z0}^2/d_{x0}^2$ where d_{z0}^2/d_{x0}^2 is the ratio of internal dipole moments squared and β is a parameter taking into account the impact of the NW on the PL emission. The

emission of the A band is expected to be perpendicular to the c-axis, i.e. to the NW axis [6]. The situation is different for the B band where no dipole orientation is forbidden.[9]

	// c-axis	⊥ c-axis
E_A	0	$\frac{m_0}{4}E_{px}$
E_B	$b^2\left(\frac{m_0}{2}E_{pz}\right)$	$a^2\left(\frac{m_0}{4}E_{px}\right)$
E_C	$a^2\left(\frac{m_0}{2}E_{pz}\right)$	$b^2\left(\frac{m_0}{4}E_{px}\right)$

Table 1: Interband momentum-matrix elements for polarization parallel and perpendicular to the c axis.[6]

The interband momentum-matrix elements of the A, B and C bands are given in Table 1 where a, b, E_{pz} and E_{px} are related to the following equations (from Ref 6):

$$a=\frac{E_2}{\sqrt{E_2^2+2\Delta_3^2}},b=\frac{\sqrt{2}\Delta_3}{\sqrt{E_2^2+2\Delta_3^2}} \tag{3}$$

$$E_{pz}=\left(\frac{m_0}{m_e^z}-1\right)\frac{\left(E_g+\Delta_{CR}+\Delta_2\right)\left(E_g+2\Delta_2\right)-2\Delta_3^2}{E_g+2\Delta_2} \tag{4}$$

$$E_{px}=\left(\frac{m_0}{m_e^t}-1\right)\frac{E_g\left[\left(E_g+\Delta_{CR}+\Delta_2\right)\left(E_g+2\Delta_2\right)-2\Delta_3^2\right]}{\left(E_g+\Delta_{CR}+\Delta_2\right)\left(E_g+\Delta_2\right)-\Delta_3^2} \tag{5}$$

with E_g the band gap, $E_2=\Delta_{CR}/2-\Delta_{SO}/6+\sqrt{\left(\Delta_{CR}+\Delta_{SO}\right)^2/4-2\Delta_{CR}\Delta_{SO}/3}$, $\Delta_2=\Delta_3=\Delta_{SO}/3$, m_e^t and m_e^z the transverse and longitudinal electron effective masses, respectively. The experimental values m^z_e=0.078 and m^t_e=0.093, recently obtained in Ref 2, are used for the calculations. As far as the B transition is concerned, the ratio of the interband momentum-matrix elements, parallel over perpendicular to the c-axis, is equal to $d_{z0}^2/d_{x0}^2=2b^2E_{pz}/a^2E_{px}$, is related to the Δ_{CR} and Δ_{SO} values and not on a symmetrical way. This ratio has been calculated for the B transition as a

function of Δ_{CR} and Δ_{SO} in the case of Wz InP. These results are reported in Fig 1 where black lines represent different values of d_{z0}^2/d_{x0}^2 .

Numerous groups have reported experimental [1,7,8,10,11] or theoretical [9,12,13] values of Δ_{CR} and Δ_{SO}. These values are reported in Fig. 1.b. Due to the symmetric nature of the equations (1) and (2), for each experimental study, two points are reported. Fig 1 reveals that the two possible solutions of equations (1) (2) provide strongly different d_{z0}^2/d_{x0}^2 ratio values for the B transition: if $\Delta_{CR}>\Delta_{SO}$, we would expect $d_{z0}^2/d_{x0}^2<0.5$, whereas $d_{z0}^2/d_{x0}^2>1$ is expected if $\Delta_{CR}>\Delta_{SO}$. As a consequence the determination of this ratio by polarized PL will conclude on the good assumption: $\Delta_{CR} > \Delta_{SO}$ or $\Delta_{SO} > \Delta_{CR}$. We would like to highlight that a strategy to determine the correct solution of equation (1) and (2) would be to assume that the Δ_{SO} value is comparable to the known bulk zinc-blende (ZB) InP Δ_{SO} value of 108 meV (from Ref 14) and attribute the second value to Δ_{CR}. However, as shown in Fig 1.b, both solutions of the equations (1) (2) lead to values which are relatively far from the known Δ_{SO} value of bulk ZB InP. As a consequence, it is difficult to use such a strategy in the present situation.

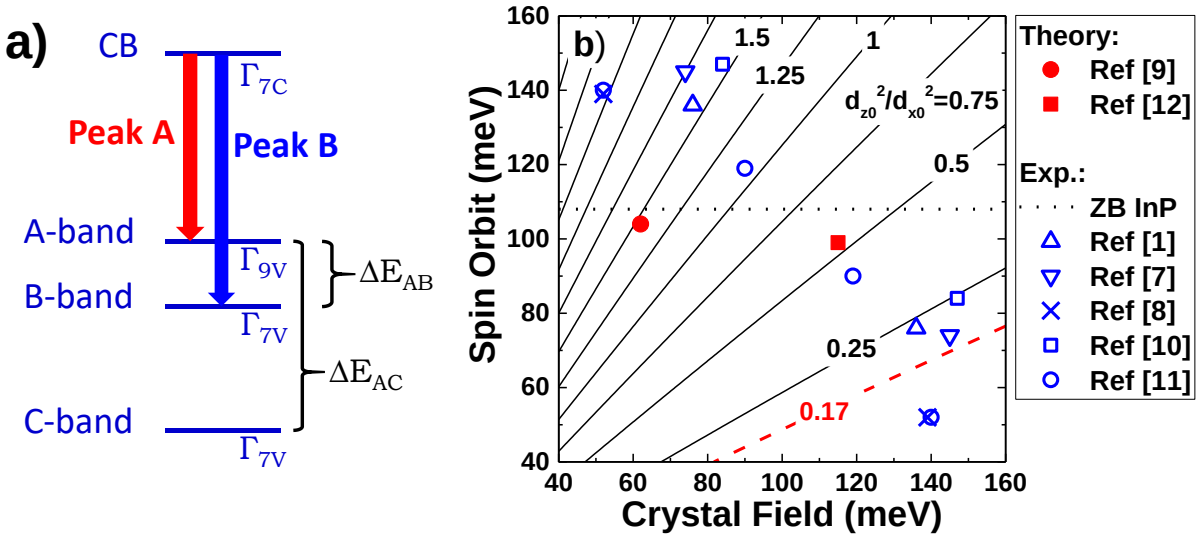

Figure 1: a) band structure of Wz InP. b) Theoretical d_{z0}^2/d_{x0}^2 ratio of the B transition as a function of Δ_{CR} and Δ_{SO}.

To investigate this issue, a Wz InP NW sample was grown on a Si(111) substrate by VLS-ssMBE using Au-In droplets as catalyst in-situ deposited at 500°C. A strong interest of this

procedure is to induce the growth of a field of vertical Wz InP NWs as detailed in Reference.[15] Two growth steps were performed at different substrate temperatures to obtain the NWs. First, the NWs were grown during 10 minutes at 380°C with an indium flux corresponding to an InP 2D layer equivalent growth rate of 1 ML/s and with a P_V/P_{III} beam equivalent pressure (BEP) ratio equal to 20 in order to produce pure Wz InP NWs.[7] To increase the NW diameter, a second growth step of 10 minutes was performed at a lower temperature (340°C) to favor the NW radial growth. The sample is composed of vertical 800 nm ± 50 nm long NWs with a constant diameter (without tapering) of 90 nm ± 5 nm and a NW density of ≈ 7 NWs per µm² (Fig. 2.a). InP NWs have been investigated by high-resolution transmission electron microscopy (HRTEM). Figure 2.b shows the dark field TEM image of a typical InP NW oriented along the [11-20] Wz zone axis. In this orientation, Wz and ZB crystal structures show two different diffraction patterns in which the spots belonging to one phase are well separated from those of the other. Therefore, a good contrast can be obtained between the two phases by selecting the spots of one of the two phases. The NW shown has a 770 nm length and a 90 nm diameter. The NW has a perfect Wz crystallographic structure during the first 620 nm length. This length corresponds to the typical size of the InP NWs after the initial 10 mn axial growth at 380°C. Then, few ZB insertions are observed in the upper part of the NW. This part is related to the axial growth of the NWs during the second growth step at 340°C. This second step is required to increase the NW diameter: the NWs have usually a 50-60 nm diameter after the first growth step.

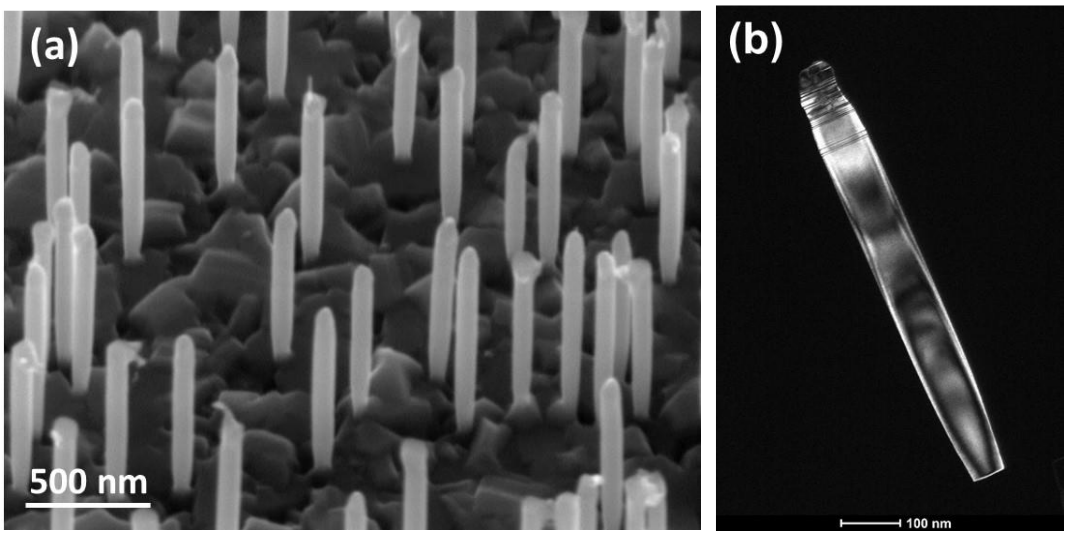

Figure 2: (a) SEM Image of the InP NWs. (b) Dark field TEM image of an InP NW.

The sample is characterized in a PL setup composed of a close cycled helium cooled cryostat, a 532 nm continuous wave (cw) diode-pumped solid-state laser and a nitrogen cooled silicon CCD detector coupled to a monochromator. The low temperature PL spectrum revealed a sharp emission at 1.492 eV, the transition energy of the A exciton in Wz InP (Figure 3).[1] At room temperature a peak (at 1.426 eV) and one shoulder (at ≈ 1.46 eV) are observed and are related to A and B transitions, respectively. The B transition is observed due to the thermal activation of the holes from the A to the B band. These results are the usual features on Wz InP NWs and confirm the Wz crystallographic phase of the NWs. The observation of the B transition at room temperature allows us to investigate its polarization resolved emission.

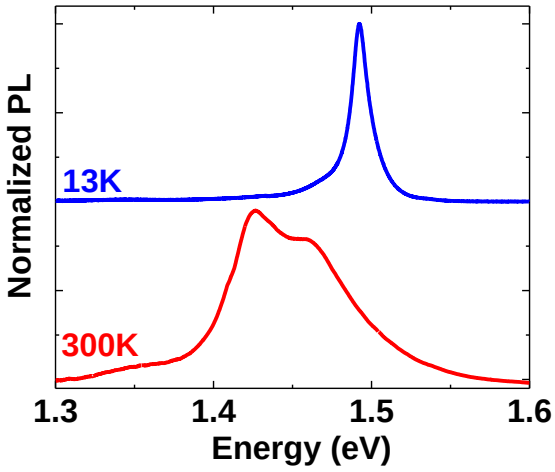

Figure 3: Normalized PL spectra of the sample at low and room temperature.

To perform this study, a micro-photoluminescence (micro-PL) setup is build using a 671 nm continuous wave (cw) diode-pumped solid-state laser as the excitation source (laser spot size of 20 µm) and an InGaAs cooled silicon CCD detector coupled to a monochromator for the detection. The micro-PL is performed on the as-grown sample with separate excitation and analysis arms: the NWs are optically pumped from the top while the collection is performed from the side of the sample using a 0.4 numerical aperture objective microscope and a polarizer. Due to the verticality of the InP NWs grown on the substrate, the collection from the side of the sample allows to investigate the orientation of the light emission as a function of the NW axis. A low resolution grating is used to decrease the polarization dependence of the setup. Moreover, correction functions are done with a tungsten lamp to remove any polarization dependence of the setup.

Fig. 4.a shows the µ-PL emission of a NW ensemble as a function of the polarizer angle from 0° (perpendicular to the NW axis) to 180° going through 90° (parallel to the NW axis). Each spectrum consists of two peaks related to the A and B band to band transitions and is fitted using the equation[16]:

$$I = \left(I_A\sqrt{E-E_g} + I_B\sqrt{E-E_g-\Delta_{AB}}\right)\exp\left(-\frac{E-E_g}{kT}\right) \quad (6)$$

where the values E_g=1406 meV, Δ_{AB}=36 meV and kT=39 meV are identical to fit all the experimental data. The high carrier temperature is probably the consequence of long lived hot carriers in small diameter NWs. A carrier temperature of 43 meV was recently reported for 72 nm-diameter Wz InP NWs during room temperature µ-PL measurements.[17] The 36 meV splitting between the A and B bands at room temperature is also in agreement with other experimental results.[1] The intensities I_A and I_B are reported in Fig.4.b. To be able to fit these experimental results a precise analysis has to be performed.

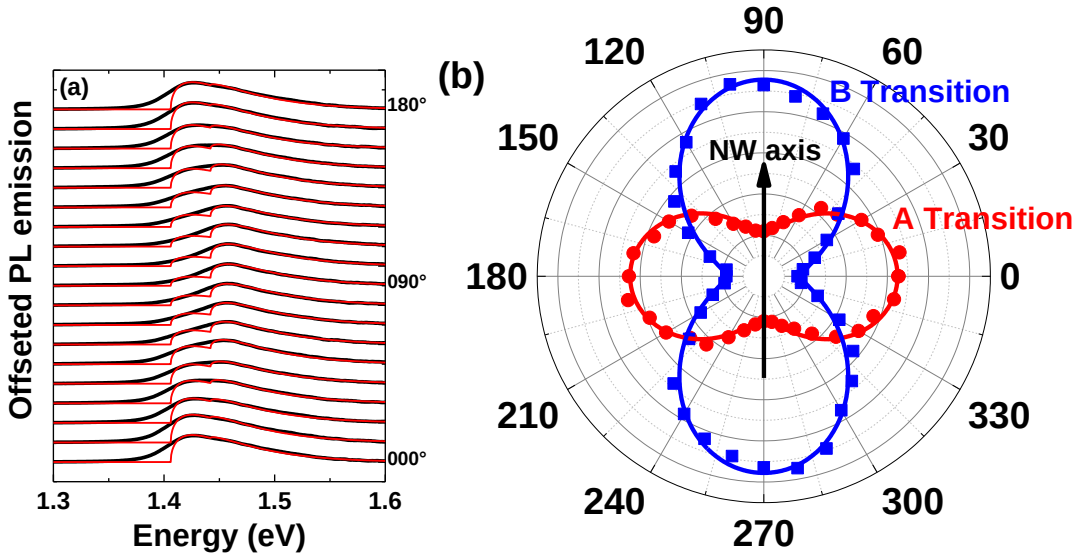

Figure 4: (a) PL spectra of the NW sample as a function of the polarization angle. PL spectra were offseted for clarity. Red curves are the fitting using Equation (3). (b) PL integrated intensity of the A and B bands as a function of the polarizer angle. NWs are aligned along the 90°-270° axis of the polarizer

The extraction of the real dipole ratio of the B transition from the experimental study is a complex problem for two reasons: 1) the emission is not localized at a specific position in the NWs and 2) the InP NWs have to be seen as a photonic structure with emission tailored through guiding and leaky modes. As a consequence the measured ratio is not the intrinsic one and the impact of the NWs on the emission has to be understood to recover the real ratio. The 90 nm-diameter InP NW field corresponds to a HE_{11} monomode structure [18] with a strong inhibition expected for the dipole oriented perpendicularly to the NW axis. The strong interest of this situation is that the screening of the dipole is independent of the dipole position in the NW plane as already shown in Ref [19] for GaAs NWs. As a consequence, the recombination rate of the dipole is independent of its in-plane position. A modification of the dipole spontaneous emission is possible along the NW axis due to the presence of the high refractive index silicon substrate. As a consequence, Finite Difference Time Domain (FDTD) calculations are performed as a function of the dipole orientation (perpendicular or parallel to the NW axis) and the dipole position along the z axis. Calculations are performed on a 800 nm long NW represented by a 90 nm in diameter cylinder on a silicon substrate. Refractive indexes of 3.42 and 3.64 are used for InP [18] and for the silicon substrate, respectively. Calculations are performed using the Opti-FDTD software.[20]

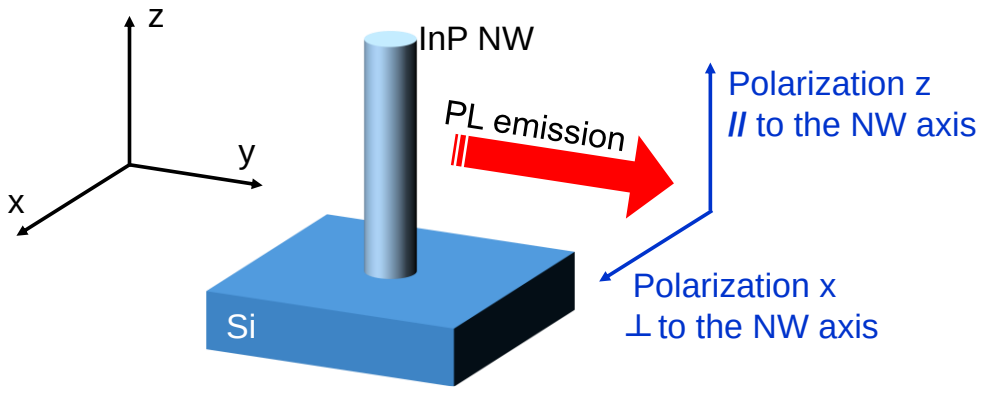

Figure 5: Schematic of the photonic structure used for the FDTD calculations.

It is also known that the far field is strongly impacted by the dipole orientation as compared to the NW axis.[18,21] This is a key issue to take into account: a modification of the far field can induce a modification of the collection efficiency in our NA=0.4 microscope objective and a wrong estimation of the intrinsic dipole ratio. The far field radiative power is calculated using the method detailed in Ref [22]. Fig. 5 shows a schematic of the calculation: z is the NW growth axis, the

polarization of the emission is investigated in the x-z plane for a dipole aligned along the NW axis (z-polarized) or perpendicular to the NW axis (x-polarized). There is also a dipole oriented perpendicularly to the NW axis along the y axis but the probability to collect photons emitted by this dipole orientation is weak as a consequence of the NA=0.4 numerical aperture.[23] The total averaged power emitted by the x-polarized (z-polarized) dipole and collected by the microscope objective is equal to [22]

$$P_{x(z)} = 2\frac{\eta}{8\lambda^2 k^2}\iint_{\left|\vec{k}_{//}\right|\le k_{NA}} dk_x.dk_z\left(\left|FT_2(H_{z(x)})\right|^2 + \frac{1}{\eta^2}\left|FT_2(E_{x(z)})\right|^2\right) \quad (7)$$

where k_{NA} is determined by the numerical aperture of the microscope objective, $\eta = \sqrt{\mu_0/\varepsilon_0}$ and FT_2 is the Fourier transform of the near field components $E_{x(z)}$ and $H_{z(x)}$. The integration is performed over the 0.4 numerical aperture of the experimental setup. The ratio $\beta = P_z/P_x$ is calculated and a value of 32 is obtained. This high value of β is explained by the strong inhibition of the dipole oriented perpendicularly to the NW axis. To take into account the NW diameter distribution observed in our sample, the same FDTD calculations are performed for NW diameters of 85 nm and 95 nm and β values of 35 and 20 are obtained, respectively. Another source of error for β could be related to the refractive index chosen in the FDTD calculations. There are no experimental value available for the Wz InP refractive index and the value of the ZB InP is used. This approximation is very usual in the literature. But to confirm that this choice has not a too strong impact on the value of β, we have also performed the same FDTD calculations with the theoretical values published by De and Pryor (using n_z=3.35 and n_x= n_y=3.83) to take into account the anisotropy of the Wz material.[24] A value $\beta = 28$ is obtained from the simulation for a 90 nm diameter NW. As a consequence, we will assume that $\beta = 30 \pm 10$.

The experimental results are fitted with the equation:

$$I(\theta) = I_0\left[cos^2(\theta) + \frac{d_{z0}^2}{d_{x0}^2}\beta sin^2(\theta)\right] \quad (8)$$

The d_{z0}^2/d_{x0}^2 ratios are extracted for the A and B bands and values of 0.01 and 0.17±0.06 are obtained, respectively. As a far as the A band is concerned, the value is very close to the theoretical one, i.e. a dipole oriented perpendicularly to the NW axis due to a forbidden transition for the polarization oriented parallel to the NW axis. Concerning the B band the most important information is that d_{z0}^2/d_{x0}^2 is smaller than one. The dashed red line in Fig. 1.b represents the position of $d_{z0}^2/d_{x0}^2 = 0.17$. It means that Δ_{CR} is bigger than Δ_{SO} for Wz InP, in agreement with the calculated values published in Ref 12 and in Ref 13 but in contradiction with Ref [9]. If we refer to the literature, a majority of Wz III-V semiconductors have a Δ_{CR} which is smaller than Δ_{SO}.[9] However, the condition $\Delta_{CR} > \Delta_{SO}$ is not exceptional and is predicted for several Wz III-V semiconductors such as GaN, GaP and InN.[9] This result allows us to confirm from our former PLE measurements that $\Delta_{CR} \approx$ 145 meV and $\Delta_{SO} \approx$ 74 meV.[7] These results lead to a Δ_{SO} value which is clearly smaller in Wz InP (74 meV) than in ZB InP (108 meV). This observation is in contradiction with the theoretical calculations of Δ_{SO} in InP polytypes where a variation of a few percent is predicted between two different crystallographic phases.[9,12,13] In both WZ and ZB configurations the nearest neighbors are tetahedrally bonded. To explain a modification of the Δ_{SO} value between the two phases, we have to assume that the interactions with the second or third nearest neighbors are not negligible.[11] The knowledge of these values is an important information to be able to perform accurate band structure calculations when Δ_{CR} and Δ_{SO} do not act on a symmetrical way. Moreover the experimental method proposed in this paper could be used for other Wz materials once the configurations $\Delta_{CR} > \Delta_{SO}$ and $\Delta_{CR} < \Delta_{SO}$ provide strongly different d_{z0}^2/d_{x0}^2 ratios.

ACKNOWLEDGMENT

This work has been supported by the Agence Nationale pour la Recherche project INSCOOP (ANR-11-NANO-012). Authors are gratefully acknowledging facilities and technological staffs from Nanolyon platform.

REFERENCES

[1] A. Zilli, M. De Luca, D. Tedeschi, H.A. Fonseka, A. Miriametro, H.H. Tan, C. Jagadish, M. Capizzi, and A. Polimeni, ACS Nano **9**, 4277 (2015).

[2] D. Tedeschi, M. De Luca, A. Granados del Aguila, Q. Gao, G. Ambrosio, M. Capizzi, H.H. Tan,

P.C.M. Christianen, C. Jagadish, and A. Polimeni, Nano Lett. **16**, 6213 (2016).

[3] N. Chauvin, A. Mavel, G. Patriarche, B. Masenelli, M. Gendry, and D. Machon, Nano Lett. **16**, 2926 (2016).

[4] G. Bulgarini, D. Dalacu, P.J. Poole, J. Lapointe, M.E. Reimer, and V. Zwiller, Appl. Phys. Lett. **105**, 191113 (2014).

[5] M. Dunaevskiy, P. Geydt, E. Lähderanta, P. Alekseev, T. Haggren, J. Kakko, H. Jiang, and H. Lipsanen, Nano Lett. **17**, 3441 (2017).

[6] S. Chuang and C. Chang, Phys. Rev. B **54**, 2491 (1996).

[7] M.H. Hadj Alouane, N. Chauvin, H. Khmissi, K. Naji, B. Ilahi, H. Maaref, G. Patriarche, M. Gendry, and C. Bru-Chevallier, Nanotechnology **24**, 35704 (2013).

[8] S. Perera, K. Pemasiri, M.A. Fickenscher, H.E. Jackson, L.M. Smith, J. Yarrison-Rice, S. Paiman, Q. Gao, H.H. Tan, and C. Jagadish, Appl. Phys. Lett. **97**, 23106 (2010).

[9] F. Bechstedt and A. Belabbes, J. Phys. Condens. Matter **25**, 273201 (2013).

[10] E. Gadret, G.O. Dias, L.C.O. Dacal, M.M. de Lima Jr., C.V.R.S. Ruffo, F. Iikawa, M.J.S.P. Brasil, T. Chiaramonte, M.A. Cotta, L.H.G. Tizei, D. Ugarte, and A. Cantarero, Phys. Rev. B **82**, 125327 (2010).

[11] S. Perera, T. Shi, M.A. Fickenscher, H.E. Jackson, L.M. Smith, J.M. Yarrison-Rice, S. Paiman, Q. Gao, H.H. Tan, and C. Jagadish, Nano Lett. **13**, 5367 (2013).

[12] J.-M. Jancu, K. Gauthron, L. Largeau, G. Patriarche, J.-C. Harmand, and P. Voisin, Appl. Phys. Lett. **97**, 41910 (2010).

[13] A. De and C.E. Pryor, Phys. Rev. B **81**, 155210 (2010).

[14] I. Vurgaftman, J.R. Meyer, and L.R. Ram-Mohan, J. Appl. Phys. **89**, 5815 (2001).

[15] A. Mavel, N. Chauvin, P. Regreny, G. Patriarche, B. Masenelli, and M. Gendry, J. Cryst. Growth **458**, 96 (2017).

[16] M. Grundmann, *The Physics of Semiconductors*, Springer (2006).

[17] D. Tedeschi, M. De Luca, H.A. Fonseka, Q. Gao, F. Mura, H.H. Tan, S. Rubini, F. Martelli, C. Jagadish, M. Capizzi, and A. Polimeni, Nano Lett. **16**, 3085 (2016).

[18] R. Paniagua-Dominguez, G. Grzela, J. Gomez Rivas, and J.A. Sanchez-Gil, Nanoscale **5**, 10582 (2013).

[19] J. Bleuse, J. Claudon, M. Creasey, N.S. Malik, J.-M. Gérard, I. Maksymov, J.-P. Hugonin, and P. Lalanne, Phys. Rev. Lett. **106**, 103601 (2011).

[20] Y. Chen, L. Zhan, J. Wu, and T. Wang, Opt. Express **22**, 2222 (2014).

[21] C. Wilhelm, A. Larrue, X. Dai, D. Migas, and C. Soci, Nanoscale **4**, 1446 (2012).

[22] J. Vuckovic, Loncar Marko, H. Mabuchi, and A. Scherer, IEEE J. Quantum Electron. **38**, 850 (2002).

[23] T.B. Hoang, L. V Titova, J.M. Yarrison-Rice, H.E. Jackson, A.O. Govorov, Y. Kim, H.J. Joyce, H.H. Tan, C. Jagadish, and L.M. Smith, Nano Lett. **7**, 588 (2007).

[24] A. De and C.E. Pryor, Phys. Rev. B **85**, 125201 (2012).